European Journal of Radiology 118 (2019) 223–230

Contents lists available at ScienceDirect

European Journal of Radiology

journal homepage: www.elsevier.com/locate/ejrad

Research article

Whole-body bone marrow DWI correlates with age, anemia, and hematopoietic activity

Tetsuya Tsujikawa[a,*], Hiroshi Oikawa[a], Toshiki Tasaki[b], Naoko Hosono[b], Hideaki Tsuyoshi[c], Yoshio Yoshida[c], Takahiro Yamauchi[b], Hirohiko Kimura[d], Hidehiko Okazawa[a]

[a] Biomedical Imaging Research Center, University of Fukui, Fukui, Japan
[b] Department of Hematology and Oncology, Faculty of Medical Sciences, University of Fukui, Fukui, Japan
[c] Department of Obstetrics and Gynecology, Faculty of Medical Sciences, University of Fukui, Fukui, Japan
[d] Department of Radiology, Faculty of Medical Sciences, University of Fukui, Fukui, Japan

ARTICLE INFO

Keywords:
Diffusion magnetic resonance imaging
Bone marrow
Age factors
Anemia
Hematopoiesis

ABSTRACT

Purpose: To identify the predictors of bone-marrow DWI signals from anthropometric, complete blood count (CBC), and C-reactive protein (CRP), and to evaluate the association with fat-content in patients.
Method: This retrospective study was approved by the institutional review board. A total of 113 consecutive tumor patients underwent whole-body PET/MRI. Apparent diffusion coefficient (ADC) and proton density fat fraction (PDFF) were measured and averaged in lumbar vertebrae (L3-5) and bilateral ilia. Due to respiratory motion, ribs were evaluated by 3-point visual scoring on DWI with b = 800 (1: invisible, 2: partially visible, 3: fully visible). The relationships between ADC/visual scores and anthropometric, CBC, CRP, and PDFF were examined. In females, the age-dependency was evaluated.
Results: Multi-regression analyses identified age as the strongest predictor of lumbar ADC (standardized coefficient: β = 0.45), followed by red cell distribution width (RDW) (β = −0.24), while age was the strongest predictor of iliac ADC (β = 0.43), followed by hemoglobin (Hb) (β = 0.22). RDW was the strongest predictor (β = 0.47) for rib visual score and age was the second (β = -0.39). ADC showed significant positive correlations with PDFF at L3-5 and ilium. Lumbar ADC showed a decreasing trend during middle age in females.
Conclusions: Age, anemia (lower Hb), and increased hematopoietic activity (higher RDW) are the predominant predictors of ADC and the visibility of red marrow on DWI. Fat-suppression methods and bone-marrow physiology in middle-aged females may have affected the measured correlations between ADC and PDFF inconsistent with previous studies.

1. Introduction

Diffusion-weighted imaging (DWI) is a quantitative functional magnetic resonance imaging (MRI) technique complementary to positron emission tomography (PET) with 2-[^{18}F]-fluoro-2-deoxy-*D*-glucose (^{18}F-FDG) [1]. Whole-body DWI with apparent diffusion coefficient (ADC) quantification is currently used for cancer staging and assessing treatment responses to diseases involving bone marrow [2–4]. Proton density fat fraction (PDFF) measurements have been used to assess hepatic steatosis [5,6], and whole-body PDFF imaging is being applied to evaluate the fat content of bone marrow in patients with benign and malignant diseases [7,8].

Bone marrow ^{18}F-FDG uptake (reflecting glucose metabolism) is reported to be associated with age, white blood cell (WBC), serum C-reactive protein (CRP), and treatment with granulocyte colony-stimulating factor (GCSF) or erythropoietin [9–13]. However, the predictive factors for bone marrow signals on DWI are mostly unknown and may have an impact on image interpretation of bone marrow when using whole-body DWI to assess disease burden and treatment response. Moreover, it has been reported that fat content in bone marrow may be

Abbreviations: PDFF, Proton density fat fraction; EPI, Echoplanar imaging; STIR, Short inversion time inversion recovery; SSRF, Spectral-spatial radiofrequency; SNR, Signal-to-noise ratio; IDEAL-IQ, Iterative decomposition of water and fat with echo asymmetry and least-squares estimation quantitation sequence; LAVA, Liver acquisition with volume acquisition; SSFSE, Single shot fast spin echo; CBC, Complete blood count; WBC, White blood cell; RBC, Red blood cell; Hb, Hemoglobin; RDW, Red cell distribution width; Plt, Platelet count; PDW, Platelet distribution width; CRP, C-reactive protein; GCSF, Granulocyte colony-stimulating factor; GFR, Glomerular filtration rate; FES, 16α-^{18}F-fluoro-17β-estradiol; FLT, 3'-deoxy-3'-^{18}F-fluorothymidine

* Corresponding author at: Biomedical Imaging Research Center, University of Fukui, 23-3 Matsuoka-Shimoaizuki, Eiheiji-cho, Fukui 910-1193, Japan.
E-mail address: awaji@u-fukui.ac.jp (T. Tsujikawa).

https://doi.org/10.1016/j.ejrad.2019.07.022
Received 1 February 2019; Received in revised form 26 May 2019; Accepted 17 July 2019

a major contributing factor to restricted diffusion in patients with myeloma [14].

The objectives of this study were twofold: first, to identify the predominant predictors for bone marrow signals on DWI from anthropometric and blood-related data including complete blood count (CBC) and CRP in patients; and second, to evaluate the association of bone marrow DWI with fat content in patients, and with age in females.

2. Material and methods

2.1. Patient population

We retrospectively reviewed the medical records of all tumor patients at diagnosis who underwent whole-body PET/MRI in our institute between February 2017 and October 2017. Patients were eligible for the study if they fulfilled the following criteria: (1) whole-body DWI and ADC maps were obtained, (2) CBC and CRP data measured within one week of the scan were available, and (3) normal renal function was established. Normal renal function is defined as an estimated glomerular filtration rate (eGFR) > 50 ml/min/1.73m^2; this condition is necessary because renal insufficiency is associated with impaired erythropoietic response to anemia. The specific PET tracer used in whole-body PET/MRI was not considered because the most significant objective in this study was to identify the predominant predictors for bone marrow signals on DWI from anthropometric and blood-related data. Patients were excluded from this study if they had bone metastasis, a hematological disorder (myeloma, leukemia, myelodysplastic syndrome, lymphoma etc.) or a previous history of chemotherapy, radiotherapy, or use of GCSF.

One hundred and six patients (92 females, 14 males; mean age = 55.5 ± 14.3 years) were identified. The details of patients and PET/MR scans are shown in Table 1. Since 3 female patients with gynecological cancer underwent PET/MR scans with ^{18}F-FDG and 16α-^{18}F-fluoro-17β-estradiol (^{18}F-FES), 2 female patients with gynecological cancer underwent pre- and post-operative ^{18}F-FDG PET/MR scans, and one male patient with lung cancer sequentially underwent 3 PET/MR scans with 3′-deoxy-3′-^{18}F-fluorothymidine (^{18}F-FLT), a total of 113 PET/MR scans (86 with ^{18}F-FDG, 19 with ^{18}F-FES, and 8 with ^{18}F-FLT) were evaluated in the present study. This retrospective study was approved by the Ethics Committee of our institute, and the requirement to obtain formal written consent was waived.

2.2. Whole-body PET/MRI

2.2.1. PET scan and Dixon-based MR-AC

Patients fasted for at least 4 h prior to an intravenous injection of 200 M Bq ^{18}F-FDG, ^{18}F-FES, or ^{18}F-FLT. Fifty minutes after the injection, patients were transferred to the whole-body simultaneous 3.0 T PET/MR scanner (Signa PET/MR, GE Healthcare, Waukesha, WI, USA). Scan protocols of PET and Dixon-based MR attenuation correction were separately described in Supplementary Method 1.

Table 1
Patients and PET/MR scans.

Disease	n	PET	Total PET/MR scans
Gynecological tumor	69	^{18}F-FDG	69 with ^{18}F-FDG
(n = 90, 90 F, 55.5 ± 14.4 yo)	16	^{18}F-FES	16 with ^{18}F-FES
	3	^{18}F-FDG + ^{18}F-FES	3 with ^{18}F-FDG, 3 with ^{18}F-FES
	2	^{18}F-FDG × 2	4 with ^{18}F-FDG
Lung cancer	5	^{18}F-FLT	5 with ^{18}F-FLT
(n = 6, 5 M1F, 56.3 ± 14.2 yo)	1	^{18}F-FLT × 3	3 with ^{18}F-FLT
Rectal cancer	5	^{18}F-FDG	5 with ^{18}F-FDG
(n = 5, 4M1F, 56.0 ± 14.3 yo)			
Head and neck cancer	5	^{18}F-FDG	5 with ^{18}F-FDG
(n = 5, 5 M, 55.8 ± 14.3 yo)			

Number of patients, gender (M: male, F: female), and mean age ± SD are shown in parentheses.
All PET/MR scans include whole-body DWI and PDFF.

2.2.2. MR sequence parameters

Additional MR sequences were acquired in the axial plane and the parameters are shown in Supplementary Table 1. DWI was performed using a single shot echoplanar imaging (EPI) sequence under free breathing (TR/TE: 5000/61 ms; b values: 0, 800 s/mm^2; FOV 576 × 345 mm; matrix 128 × 128; slice thickness/overlap: 6/0 mm; 40 image/bed; imaging time: 2 min 30 s). A short inversion time inversion recovery (STIR) pre-pulse was used for fat suppression in whole-body DWI because of its insensitivity to magnetic field inhomogeneity [15], and a selective water excitation (spectral-spatial radiofrequency, SSRF) pre-pulse was used together with STIR to yield higher signal-to-noise ratio (SNR) in the abdomen and pelvis [16] (Fig. 1A). PDFF quantification was performed using an iterative decomposition of water and fat with echo asymmetry and least-squares estimation quantitation sequence (IDEAL-IQ) (a quantitative chemical shift-based water-fat separation method with a multiecho gradient echo [17]; TR/TEs: 7.1/0.9 − 5.3 ms, 6 echoes; FOV 500 × 300 mm; matrix 256 × 192; slice thickness/overlap: 6/0 mm; 34 image/bed; imaging time: 20 s), T1-weighted imaging was performed using a liver acquisition with volume acquisition (LAVA-Flex) sequence (3D spoiled gradient echo; TR/TE1/TE2: 4.4/1.3/2.2 ms; FOV 500 × 400 mm; matrix 300 × 200; slice thickness/overlap: 4/2 mm; 120 image/slab; imaging time: 13 s), and T2-weighted imaging was performed using a single shot fast spin echo (SSFSE) sequence (TR/TE: 1600/80 ms; FOV 500 × 300 mm; matrix 384 × 256; slice thickness/overlap: 6/0 mm; 40 image/bed; imaging time: 1 min 3 s). ADC and PDFF maps were generated and used in subsequent assessments.

2.3. Quantitative image assessment

MR images were transferred to the GE workstation (AW 4.6) and evaluated with matched spatial registration (Fig. 1B). Circular regions of interest (ROIs) with a fixed diameter of 20 mm were placed on lumbar vertebrae (L3-5) and bilateral posterior iliac crests. ADC and PDFF were measured and averaged in L3-5 and iliac bones by the agreement of an experienced radiologist and hematologist (TeT and ToT with 17 and 15 years of experience, respectively). Due to respiratory motion, a 3-point visual scoring on maximum intensity projection (MIP) image of DWI with b = 800 was used to evaluate the ribs (Fig. 1C). Score 1 was assigned to images in which ribs were invisible, score 2 to images in which ribs were partially visible, and score 3 to images in which ribs were fully visible. The relationships between ADC/rib visual scores and anthropometric, blood-related data and PDFF were examined. Anthropometric data included age, height, and weight. Gender was excluded as a factor due to the predominance of female patients in this study. Blood-related data evaluated in this study are shown in Table 2 with the corresponding ranges that are considered normal in our hospital.

2.4. Statistical analysis

Stepwise multiple linear regression analysis was performed to find the predominant predictive factors for ADC and rib visual scores from anthropometric and blood-related data. Regression analyses between ADCs and the top 2 predictors were performed using Pearson's correlation coefficient, and between rib visual scores and the top 2 predictors using Spearman's correlation coefficient. In group comparisons of the rib visual score, differences were assessed using a one-way analysis of variance (ANOVA) with a post hoc Bonferroni test. Regression analyses of ADC with PDFF were performed using Pearson's correlation coefficient. To evaluate the age-dependency of ADC and PDFF in female patients, linear and nonlinear (quadratic) regression analyses of age

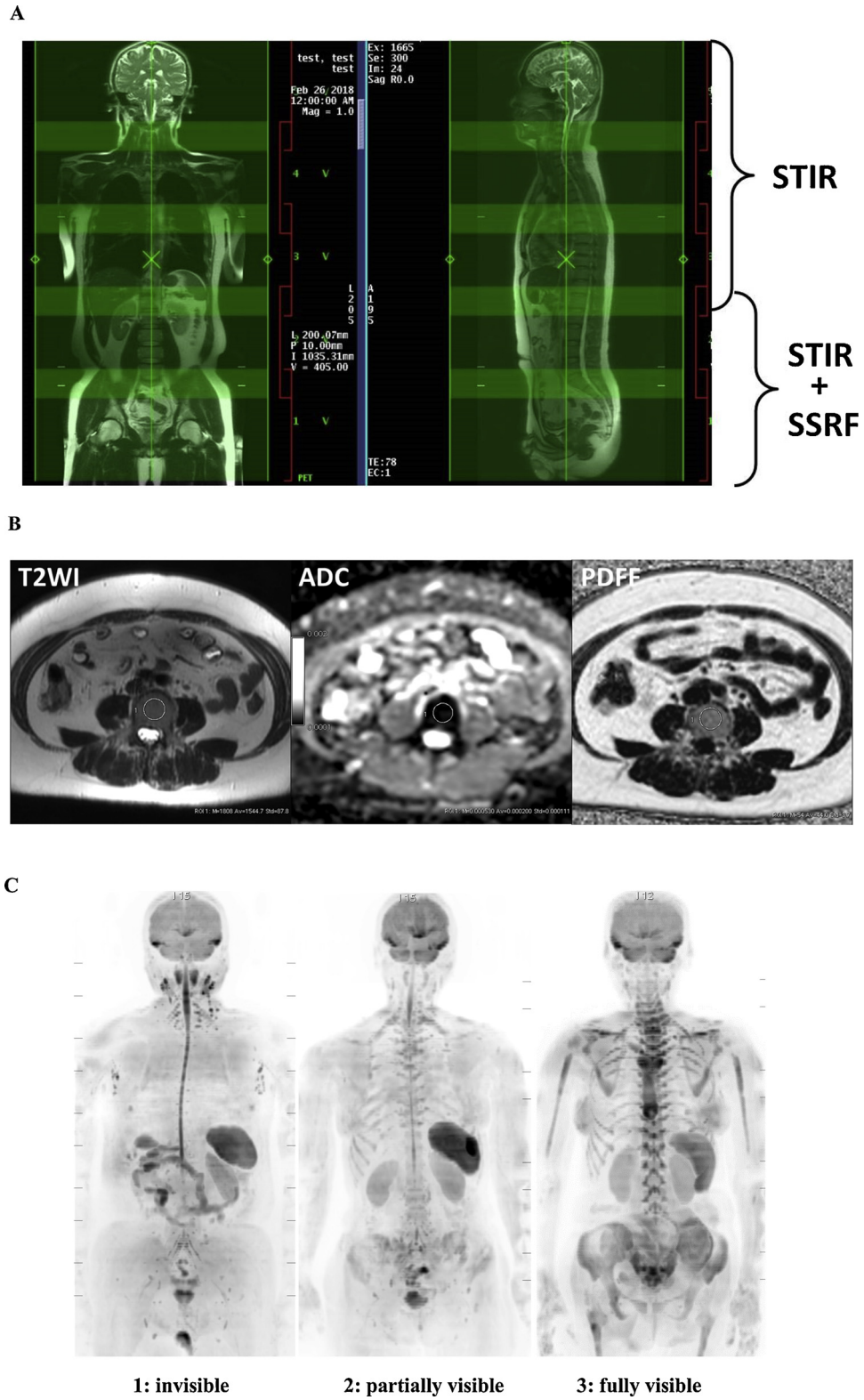

Fig. 1. Fat suppression methods at each body part in whole-body DWI (A), ROI placement on MR images (B), and 3-point visual scoring of bone marrow on maximum intensity projection DWI images with b = 800 (C).

with lumbar ADC and PDFF were performed. All statistical analyses were performed using SPSS statistics version 22 and GraphPad Prism version 6. $p < 0.05$ was considered to be significant.

3. Results

3.1. Predictor of bone marrow ADC and visual scores

Bone marrow ADCs and the ranges for each region are presented with PDFF in Table 3. The results of multiple regression analyses to

Table 2
Blood data evaluated in this study.

CBC	Abbreviation	Normal range
White blood cell	WBC	3.3 − 8.6 × 10^3 /μL
Hemoglobin	Hb	13.7 − 16.8 g/dL
Red cell distribution width	RDW	11.0 − 15.0%
Platelet count	Plt	158 − 348 × 10^3 /μL
Platelet distribution width	PDW	15.0 − 17.0%
Serum C-reactive protein	CRP	0 − 0.14 mg/dL

Table 3
Regional ADCs and PDFFs.

Region	ADC (mm^2/s)	PDFF (%)
Third lumbar vertebra (L3)	487 ± 144 (226–926)	44.5 ± 13.8 (13.9–78.1)
Fourth lumbar vertebra (L4)	463 ± 107 (225–787)	45.0 ± 14.0 (15.5–88.4)
Fifth lumbar vertebra (L5)	470 ± 122 (230–741)	45.2 ± 13.8 (14.1–76.7)
Average (L3-5)	473 ± 111 (228–771)	44.9 ± 13.5 (15.1–80.5)
Right posterior iliac crest	466 ± 126 (162–875)	60.0 ± 16.4 (24.7–88.4)
Left posterior iliac crest	471 ± 123 (214–891)	59.9 ± 16.6 (24.4–91.4)
Average (bilateral)	469 ± 119 (210–851)	60.0 ± 16.3 (25.3–89.1)

Values are mean ± SD with ranges in parentheses.

identify the predictors for bone marrow DWI are shown in Table 4. Age was the strongest predictor of lumbar ADC (standardized coefficient: β = 0.45, p < 0.0001), followed by red cell distribution width (RDW) (β = -0.24, p < 0.05). Age was the strongest predictor of iliac ADC (β = 0.43, p < 0.0001), followed by hemoglobin (Hb) (β = 0.22, p < 0.05). Fig. 2 shows the correlations between ADCs and the top 2 predictive factors. Lumbar ADC had a positive correlation with age (r = 0.39, p < 0.0001) and a negative correlation with RDW (r = -0.31, p < 0.005) (Fig. 2A and B, respectively). Iliac ADC had positive correlations with age and Hb (r = 0.39, p < 0.0001, and r = 0.28, p < 0.005, respectively) (Fig. 2C and D, respectively). Regarding the visual evaluation of the ribs, RDW was the strongest predictor of visual score (β = 0.47, p < 0.0001), followed by age (β = -0.39, p < 0.0001) (Table 4). In group comparisons, RDW was significantly higher in the score 3 group than in the score 1 and 2 groups (p < 0.005 and p < 0.01, respectively), and the score 3 group was significantly younger than the score 1 group (p < 0.005) (Fig. 3).

3.2. Representative case

Fig. 4 shows the pre- and postoperative DWI, ADC map, and PDFF of a 39-year-old woman with endometrial cancer (FIGO stage IB, histological grade 1). Bone marrow showed high signal intensity on preoperative DWI (Fig. 4A). Preoperative ADC and PDFF of L3-5 were 294.7 × 10^{-6} mm^2/s and 22.7%, respectively, and those of the ilium were 341.5 × 10^{-6} mm^2/sec and 35.7%, respectively. Preoperative blood data showed moderate anemia (Hb = 7.4 g/dL, WBC = 5.6 × 10^3 /μL, Plt = 357 × 10^3 /μL, and CRP = 0.06 mg/dL) and elevated RDW of 21%. On the other hand, the high signal intensity of bone marrow disappeared on postoperative DWI (Fig. 4B). The postoperative ADC and PDFF of L3-5 were 448.0 × 10^{-6} mm^2/sec and 42.0%, respectively, while those of the ilium were 473.5 × 10^{-6} mm^2/sec and 50.1%, respectively. Postoperative blood data showed the correction of anemia (Hb = 13.0 g/dL, WBC = 5.8 × 10^3 /μL, Plt = 330 × 10^3 /μL, and CRP = 0.16 mg/dL) and normalized RDW of 14.9%).

3.3. Correlation of bone marrow ADC with PDFF

ADC and PDFF showed positive correlations at L3-5 and the ilium (Pearson's r = 0.57, p < 0.0001 and r = 0.54, p < 0.0001, respectively) (Fig. 5A and B, respectively).

3.4. Correlation of age with lumbar ADC and PDFF in females

Fig. 6 shows linear and nonlinear regressions between age and lumbar ADC/ PDFF in 92 female patients. Although age and lumbar ADC showed a significant positive correlation (p < 0.0001), nonlinear regression showed a slightly better fit (r = 0.40) than did linear regression (r = 0.39) (Fig. 6A). Age and lumbar PDFF showed a significant positive correlation (p < 0.0001), and there was no difference in goodness of fit (r = 0.55) between linear and nonlinear regressions (Fig. 6B).

4. Discussion

To the best of our knowledge, this is the first study based on a multiple regression analysis that has clearly identified the predictive factors for bone marrow signals on whole-body DWI in anthropometric and blood-related data including CBC and CRP. Younger age, lower Hb (anemia), and higher RDW (increased hematopoietic activity) were the predominant predictors of higher visibility and lower ADC of bone marrow in DWI. Though some of these results are consistent with the findings of previous studies, some are not.

The age-dependence of bone marrow visibility on DWI was consistent with recent findings by Lavdas et al. and Cui et al. involving healthy volunteers [18,19] and by Chen et al. involving female patients [20]. They reported that the hyper-intensity of bone marrow on DWI was more frequently observed in young females. Female patients with gynecological tumors accounted for the majority of the patient population in this study (Table 1). The association of lower Hb levels with higher bone marrow visibility on DWI was also consistent with the report of Chen et al., which showed an association between high DWI signal in pelvic bone marrow and anemia in female patients [20]. The present study included many patients with gynecological tumors who were more likely to have microcytic hypochromic (iron-deficiency) anemia due to genital bleeding. In addition to age and Hb, RDW was the third predominant predictor of bone marrow signals on DWI. RDW is a measure of the range of variations in red blood cell (RBC) volumes. Higher RDW values indicate greater size variations. In the healing process of anemia, small-sized RBCs and premature large-sized reticulocytes released from red bone marrow appear in peripheral blood and result in high RDW, which means that RDW can offer an indirect

Table 4
Top 2 Predictors of Bone Marrow ADC and Visual Score.

Parameters	Lumbar ADC	Iliac ADC	Rib visual score
The strongest predictor	Age	Age	RDW
β	0.45 (p < 0.0001)	0.43 (p < 0.0001)	0.47 (p < 0.0001)
r	0.39 (p < 0.0001)	0.39 (p < 0.0001)	0.42 (p < 0.0001)
2nd strongest predictor	RDW	Hb	Age
β	−0.24 (p < 0.05)	0.22 (p < 0.05)	−0.39 (p < 0.0001)
r	−0.31 (p < 0.005)	0.28 (p < 0.005)	−0.37 (p < 0.0001)-

β: standardized coefficient calculated by a stepwise regression.
r: Pearson's correlation coefficient for ADCs and Spearman's correlation coefficient for visual score.

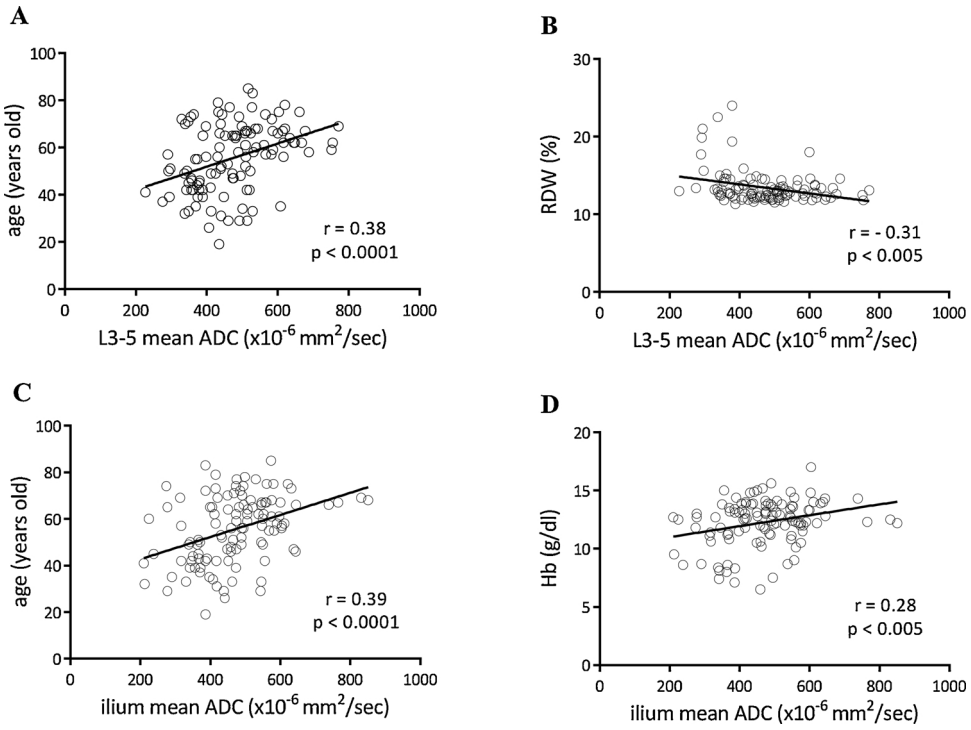

Fig. 2. Correlation between bone marrow ADCs and top 2 predictive factors.
Regression lines are shown with Pearson's correlation coefficients (r) and associated p values.

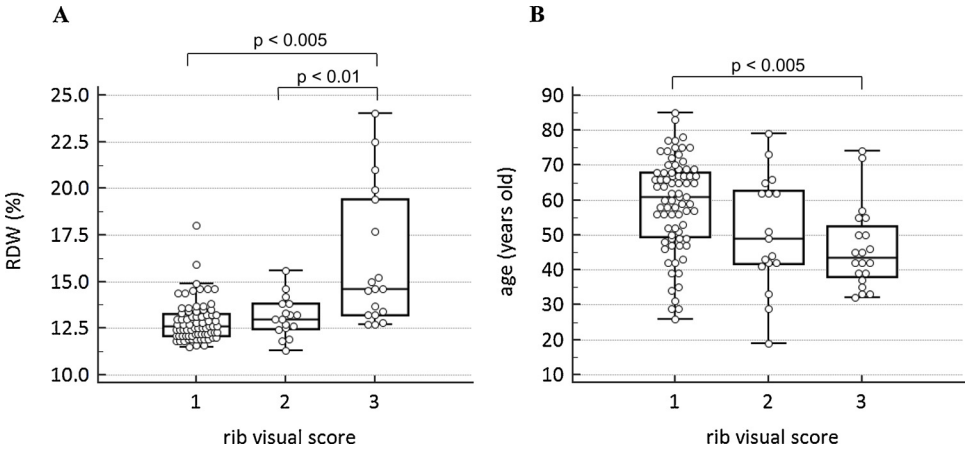

Fig. 3. Box-and-whisker plots of top 2 predictive factors for rib visual scores.
Significance for group comparisons is shown with associated p values.

measure of the hematopoietic activity of red bone marrow. Since normal renal function (eGFR > 50 ml/min/1.73m^2) was one of the inclusion criteria in the present study, patients had a low potential for nephrogenic anemia and appeared to have erythropoietin-stimulated, anemia-responsive hematopoiesis. High visibility of bone marrow on DWI thus serves as a useful indicator of anemia (low Hb) and the anemia-responsive hematopoiesis in red bone marrow (high RDW) in daily practice.

The findings in this study concerning bone marrow ADC at lumbar vertebrae and ilium are inconsistent with previous reports. In the present study, bone marrow ADCs positively correlated with age and PDFF (Fig. 2A, C, and Fig. 5A, B, respectively). Although the positive correlation between bone marrow ADC and PDFF was previously reported by Ueda et al. [21], other studies showed a negative correlation of bone marrow ADC with age and PDFF [18–20,22,23]. This negative correlation of bone marrow ADC with age and PDFF has been considered consistent with the histologic changes that take place when red marrow converts to yellow marrow; that is, increased lipid deposition along reticulum cells and trabeculae limits hematopoietic marrow and water content in relation to the proportion of fat, therefore decreasing the diffusivity of water molecules and reducing the ADC [24].

A possible cause of the discrepancy with previous results is the different fat-suppression technique used for whole-body DWI in this study. Several vendor-specific fat-suppression techniques are available for 3 T MR imaging systems [25], and some techniques can be combined with others to increase SNR and to obtain more robust fat-suppression. An STIR pre-pulse is most commonly used for fat suppression in whole-body DWI because the method is relatively insensitive to field inhomogeneities and can be used near metal and over the large fields-of-view suitable for whole-body imaging [15]. In the present study, an SSFP water excitation pre-pulse was used together with STIR to yield higher SNR at the abdomen and pelvis, including the lumbar vertebrae and ilium (Fig. 1A). Differences in ADC measurements have been reported when different fat-suppression techniques were used in breast

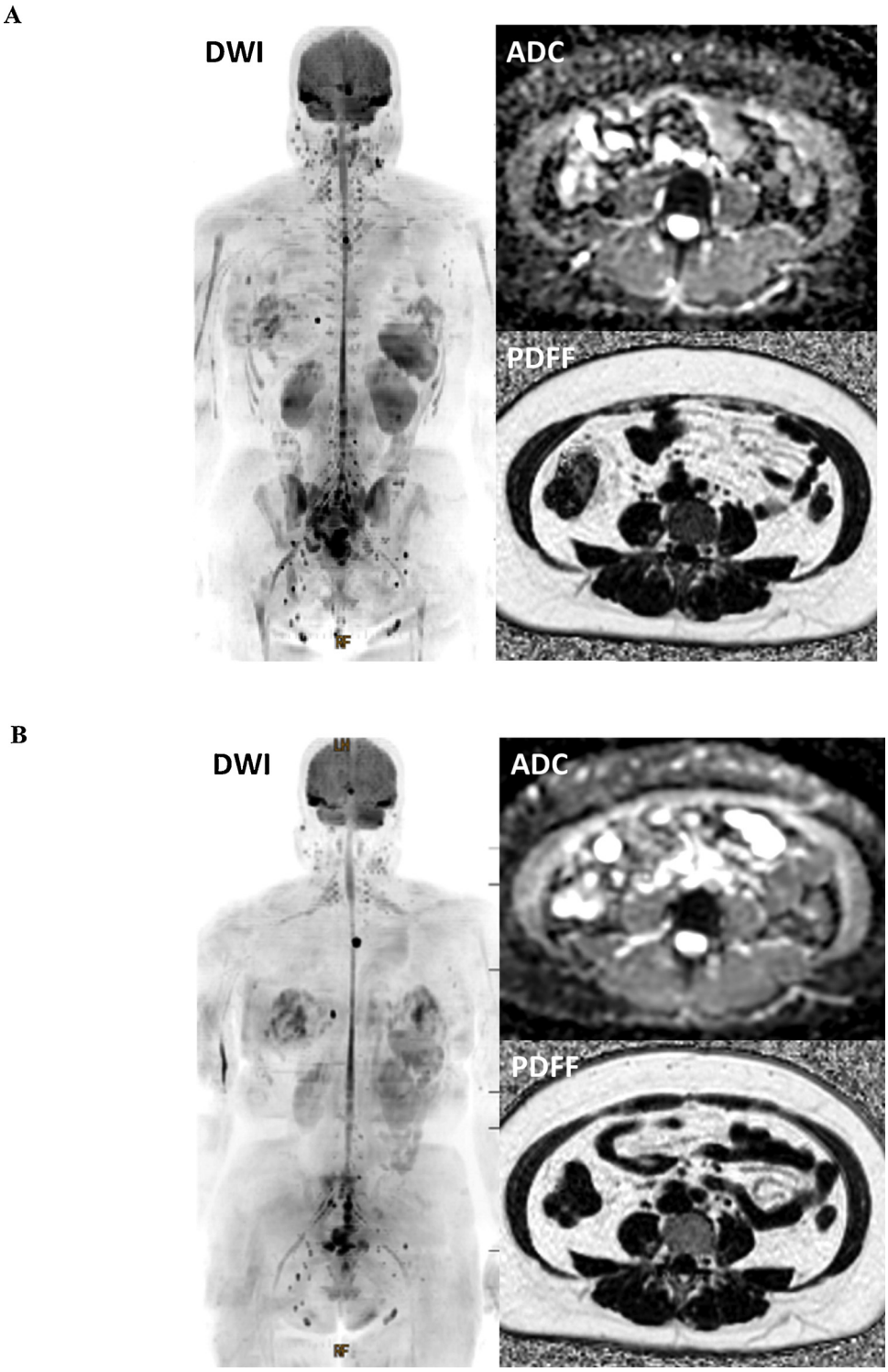

Fig. 4. A 39-year-old woman with endometrial cancer (FIGO stage IB, grade 1).
Pre- (A) and postoperative (B) whole-body DWIs are shown as maximum intensity projection images with ADC map and PDFF.

MR imaging [26,27]. It is highly likely that there are similar differences in ADC measurements of bone marrow rich in fat content.

Furthermore, Dieckmeyer et al. recently reported the confounding effect of residual fat in ADC measurements of the vertebral bone marrow water component [28]. They showed a strong underestimation of ADC that increases with PDFF, which means that the true diffusion rate of water molecules in lumbar vertebrae could be much higher than expected in the elderly. In addition, the changes with age in osseous composition (trabeculation) might have affected our results. Red bone marrow atrophy and trabecular bone loss are more evident after 40 years of age and in women, probably due to estrogen deficiency and osteoporosis [29]. Hematopoietic marrow is confined within the spaces defined by the trabeculae and supported by reticulum cells and fat cells. If these trabeculae and fat cause lower water diffusion, the trabecular bone loss can increase bone marrow ADC in the elderly. The positive correlations between bone marrow ADC and PDFF in lumbar vertebrae and ilium reported in this study are not necessarily wrong; ADC measurements are perhaps more accurately performed in DWI using the

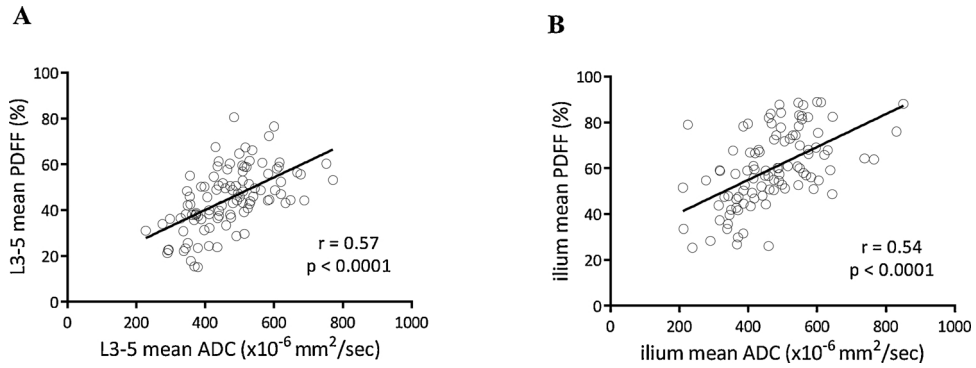

Fig. 5. Correlation between bone marrow ADCs and PDFF.
Regression lines are shown with Pearson's correlation coefficients (r) and associated p values.

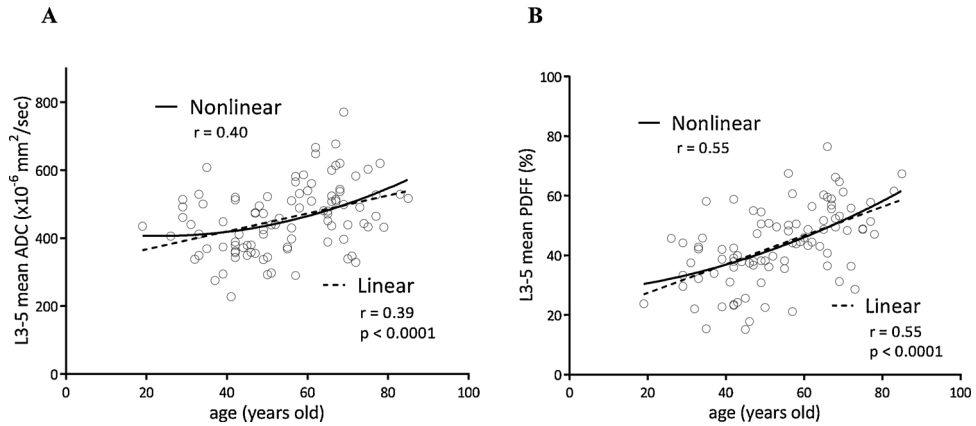

Fig. 6. Correlation of age with lumbar ADC (A) and PDFF (B) in females.
Linear and nonlinear regression lines are shown with correlation coefficients (r) and associated p values.

combination of STIR and SSFP employed in this study. In that case, the DWI signal intensity of red bone marrow increases when the water proton mobility is restricted by hyper-cellularity due to increased hematopoiesis. These results require further validation with a larger patient population, different DWI protocols, and different MRI venders.

Whole-body bone marrows contain hematopoietic cells at birth (red marrow); these are gradually replaced by fat tissue (yellow marrow), and the physiological conversion is completed by age 25. Red marrow is replaced by yellow marrow proximally to the axial skeleton. Lumbar vertebral fat content (PDFF) increased with age (Fig. 6B) and the result was consistent with the latest report of Schmeel et al. [8]. Although the youngest patient whose lumbar ADCs were measured in this study was a 19-year-old female, Tschischka et al. recently reported that the mean ADC of lumbar vertebrae in healthy children (n = 49, mean age = 10.2 ± 4.7yo) was 600 ± 90 × 10^{-6} mm^2/sec [30]. Plotting their data on Fig. 6A and performing a nonlinear regression, a decreasing trend of lumbar ADC becomes clear during middle age (Supplementary Fig. 1). These results suggest that a straight linear relationship between age and red bone-marrow ADC throughout life may not be suitable for accurately reflecting the bone marrow physiology. Perimenopausal status and/or pathophysiological responses (red marrow reconversion) to anemia might influence the bone marrow physiology, illustrated by the decreasing trend in ADC during middle age. These results require further validation with functional and molecular PET/MR imaging of bone marrow.

Our study had two limitations. First, although the predictive factors for bone marrow signals on DWI might be gender dependent [18], the gender difference was not evaluated because the study population mainly consisted of women (with gynecological tumors). A larger number of male patients are required for the evaluation of the gender difference in future research. Second, data collection allowed patients with CBC and CRP measured within one week of the scan. These values can vary within days (especially CRP), better would have been blood data from the same day.

In conclusion, age, anemia (lower Hb), and increased hematopoietic activity (higher RDW) are the predominant predictors of ADC and the visibility of bone marrow DWI. ADC showed significant positive correlations with PDFF at lumbar vertebrae and ilium in this study. Fat-suppression methods used in this study, perimenopausal status and/or pathophysiological responses to anemia may have affected the measured correlations of ADC with age and PDFF, and caused inconsistencies with previous studies. Further research is required to assess the effects of fat-suppression and perimenopausal pathophysiology on bone marrow DWI signals with a larger patient population, different DWI protocols, and additional functional PET/MR imaging.

Author statement

All authors have approved the final article.

Funding

This study was partly funded by Takeda Science Foundation.

Declaration of Competing Interest

The authors declare that they have no known competing financial interests or personal relationships that could have appeared to influence the work reported in this paper.

Appendix A. Supplementary data

Supplementary material related to this article can be found, in the online version, at doi:https://doi.org/10.1016/j.ejrad.2019.07.022.

References

[1] T.C. Kwee, T. Takahara, R. Ochiai, D.M. Koh, Y. Ohno, K. Nakanishi, T. Niwa, T.L. Chenevert, P.R. Luijten, A. Alavi, Complementary roles of whole-body diffusion-weighted MRI and ^{18}F-FDG PET: the state of the art and potential applications, J. Nucl. Med. 51 (10) (2010) 1549–1558.

[2] A.R. Padhani, D.M. Koh, D.J. Collins, Whole-body diffusion-weighted MR imaging in cancer: current status and research directions, Radiology 261 (3) (2011) 700–718.

[3] C. Lin, A. Luciani, E. Itti, T. El-Gnaoui, A. Vignaud, P. Beaussart, S.J. Lin, K. Belhadj, P. Brugieres, E. Evangelista, C. Haioun, M. Meignan, A. Rahmouni, Whole-body diffusion-weighted magnetic resonance imaging with apparent diffusion coefficient mapping for staging patients with diffuse large B-cell lymphoma, Eur. Radiol. 20 (8) (2010) 2027–2038.

[4] S.L. Giles, C. Messiou, D.J. Collins, V.A. Morgan, C.J. Simpkin, S. West, F.E. Davies, G.J. Morgan, N.M. deSouza, Whole-body diffusion-weighted MR imaging for assessment of treatment response in myeloma, Radiology 271 (3) (2014) 785–794.

[5] I.S. Idilman, H. Aniktar, R. Idilman, G. Kabacam, B. Savas, A. Elhan, A. Celik, K. Bahar, M. Karcaaltincaba, Hepatic steatosis: quantification by proton density fat fraction with MR imaging versus liver biopsy, Radiology 267 (3) (2013) 767–775.

[6] S.D. Serai, J.R. Dillman, A.T. Trout, Proton density fat fraction measurements at 1.5-and 3-T hepatic MR imaging: same-day agreement among readers and across two imager manufacturers, Radiology 284 (1) (2017) 244–254.

[7] J.P. Kuhn, D. Hernando, P.J. Meffert, S. Reeder, N. Hosten, R. Laqua, A. Steveling, S. Ender, H. Schroder, D.T. Pillich, Proton-density fat fraction and simultaneous R2*estimation as an MRI tool for assessment of osteoporosis, Eur. Radiol. 23 (12) (2013) 3432–3439.

[8] F.C. Schmeel, J.A. Luetkens, P.J. Wagenhauser, M. Meier-Schroers, D.L. Kuetting, A. Feisst, J. Gieseke, L.C. Schmeel, F. Traber, H.H. Schild, G.M. Kukuk, Proton density fat fraction (PDFF) MRI for differentiation of benign and malignant vertebral lesions, Eur. Radiol. 28 (6) (2018) 2397–2405.

[9] C.Z. Fan, M. Hernandez-Pampaloni, M. Houseni, W. Chamroonrat, S. Basu, R. Kumar, S. Dadparvar, D.A. Torigian, A. Alavi, Age-related changes in the metabolic activity and distribution of the red marrow as demonstrated by 2-Deoxy-2-[F-18]fluoro-D-glucose-positron emission tomography, Mol. Imaging Biol. 9 (5) (2007) 300–307.

[10] Y. Murata, K. Kubota, M. Yukihiro, K. Ito, H. Watanabe, H. Shibuya, Correlations between F-18-FDG uptake by bone marrow and hematological parameters: measurements by PET/CT, Nucl. Med. Biol. 33 (8) (2006) 999–1004.

[11] K. Inoue, R. Goto, K. Okada, S. Kinomura, H. Fukuda, A bone marrow F-18 FDG uptake exceeding the liver uptake may indicate bone marrow hyperactivity, Ann. Nucl. Med. 23 (7) (2009) 643–649.

[12] Y. Sugawara, S.J. Fisher, K.R. Zasadny, P.V. Kison, L.H. Baker, R.L. Wahl, Preclinical and clinical studies of bone marrow uptake of fluorine-18-fluorodeoxyglucose with or without granulocyte colony-stimulating factor during chemotherapy, J. Clin. Oncol. 16 (1) (1998) 173–180.

[13] T.M. Blodgett, J.T. Ames, F.S. Torok, B.M. McCook, C.C. Meltzer, Diffuse bone marrow uptake on whole-body F-18 fluorodeoxyglucose positron emission tomography in a patient taking recombinant erythropoietin, Clin. Nucl. Med. 29 (3) (2004) 161–163.

[14] C. Messiou, S. Giles, D.J. Collins, S. West, F.E. Davies, G.J. Morgan, N.M. Desouza, Assessing response of myeloma bone disease with diffusion-weighted MRI, Br. J. Radiol. 85 (1020) (2012) E1198–E1203.

[15] T. Takahara, Y. Imai, T. Yamashita, S. Yasuda, S. Nasu, M. Van Cauteren, Diffusion weighted whole body imaging with background body signal suppression (DWIBS): technical improvement using free breathing, STIR and high resolution 3D display, Radiat. Med. 22 (4) (2004) 275–282.

[16] C.H. Meyer, J.M. Pauly, A. Macovski, D.G. Nishimura, Simultaneous spatial and spectral selective excitation, Magn. Reson. Med. 15 (2) (1990) 287–304.

[17] H. Yu, A. Shimakawa, C.D. Hines, C.A. McKenzie, G. Hamilton, C.B. Sirlin, J.H. Brittain, S.B. Reeder, Combination of complex-based and magnitude-based multiecho water-fat separation for accurate quantification of fat-fraction, Magn. Reson. Med. 66 (1) (2011) 199–206.

[18] I. Lavdas, A.G. Rockall, F. Castelli, R.S. Sandhu, A. Papadaki, L. Honeyfield, A.D. Waldman, E.O. Aboagye, Apparent diffusion coefficient of normal abdominal organs and bone marrow from whole-body DWI at 1.5 t: the effect of sex and age, Am. J. Roentgenol. 205 (2) (2015) 242–250.

[19] F.Z. Cui, J.L. Cui, S.L. Wang, H. Yu, Y.C. Sun, N. Zhao, S.J. Cui, Signal characteristics of normal adult bone marrow in whole-body diffusion-weighted imaging, Acta Radiol. 57 (10) (2016) 1230–1237.

[20] Y.Y. Chen, C.L. Wu, S.H. Shen, High signal in bone marrow on diffusion-weighted imaging of female pelvis: correlation with Anemia and fibroid-associated symptoms, J. Magn. Reson. Imaging 48 (4) (2018) 1024–1033.

[21] Y. Ueda, T. Miyati, N. Ohno, Y. Motono, M. Hara, Y. Shibamoto, H. Kasai, H. Kawamitsu, K. Matsubara, Apparent diffusion coefficient and fractional anisotropy in the vertebral bone marrow, J. Magn. Reson. Imaging 31 (3) (2010) 632–635.

[22] J. Herrmann, N. Krstin, B.P. Schoennagel, M. Sornsakrin, T. Derlin, J.D. Busch, K.U. Petersen, J. Graessner, G. Adam, C.R. Habermann, Age-related distribution of vertebral bone-marrow diffusivity, Eur. J. Radiol. 81 (12) (2012) 4046–4049.

[23] C. Schraml, M. Schmid, S. Gatidis, H. Schmidt, C. la Fougere, K. Nikolaou, N.F. Schwenzer, Multiparametric analysis of bone marrow in cancer patients using simultaneous PET/MR imaging: correlation of fat fraction, diffusivity, metabolic activity, and anthropometric data, J. Magn. Reson. Imaging 42 (4) (2015) 1048–1056.

[24] Y. Nonomura, M. Yasumoto, R. Yoshimura, K. Haraguchi, S. Ito, T. Akashi, I. Ohashi, Relationship between bone marrow cellularity and apparent diffusion coefficient, J. Magn. Reson. Imaging 13 (5) (2001) 757–760.

[25] F. Del Grande, F. Santini, D.A. Herzka, M.R. Aro, C.W. Dean, G.E. Gold, J.A. Carrino, Fat-suppression techniques for 3-T MR imaging of the musculoskeletal system, Radiographics 34 (1) (2014) 217–233.

[26] E. Wenkel, C. Geppert, R. Schulz-Wendtland, M. Uder, B. Kiefer, W. Bautz, R. Janka, Diffusion weighted imaging in breast MRI: comparison of two different pulse sequences, Acad. Radiol. 14 (9) (2007) 1077–1083.

[27] P. Baron, M.D. Dorrius, P. Kappert, M. Oudkerk, P.E. Sijens, Diffusion-weighted imaging of normal fibroglandular breast tissue: influence of microperfusion and fat suppression technique on the apparent diffusion coefficient, NMR Biomed. 23 (4) (2010) 399–405.

[28] M. Dieckmeyer, S. Ruschke, H. Eggers, H. Kooijman, E.J. Rummeny, J.S. Kirschke, T. Baum, D.C. Karampinos, ADC quantification of the vertebral bone marrow water component: removing the confounding effect of residual fat, Magn. Reson. Med. 78 (4) (2017) 1432–1441.

[29] D. Schellinger, C.S. Lin, D. Fertikh, J.S. Lee, W.C. Lauerman, F. Henderson, B. Davis, Normal lumbar vertebrae: anatomic, age, and sex variance in subjects at proton MR spectroscopy - initial experience, Radiology 215 (3) (2000) 910–916.

[30] A. Tschischka, C. Schleich, J. Boos, M. Eichner, J. Schaper, J. Aissa, G. Antoch, D. Klee, Age-related apparent diffusion coefficients of lumbar vertebrae in healthy children at 1.5 T, Pediatr. Radiol. 48 (7) (2018) 1008–1012.